

**Prospects for a polar-molecular-ion optical probe of varying proton-electron mass ratio**Mark G. Kokish,<sup>1</sup> Patrick R. Stollenwerk,<sup>1</sup> Masatoshi Kajita,<sup>2</sup> and Brian C. Odom<sup>1,\*</sup><sup>1</sup>*Department of Physics and Astronomy, Northwestern University, Evanston, Illinois 60208, USA*<sup>2</sup>*National Institute of Information and Communications Technology, Koganei, Tokyo 184-8795, Japan*

(Received 23 April 2018; published 29 November 2018)

Molecules with deep vibrational potential wells provide optical intervals sensitive to variation in the proton-electron mass ratio ( $\mu$ ). On one hand, polar molecules are of interest since optical state preparation techniques have been demonstrated for such species. On the other hand, it might be assumed that polar species are unfavorable candidates, because typical molecule-frame dipole moments reduce vibrational state lifetimes and cause large polarizabilities and associated Stark shifts. Here, we consider single-photon spectroscopy on a vibrational overtone transition of the polar species  $\text{TeH}^+$ , which is of practical interest because its diagonal Franck-Condon factors should allow rapid state preparation by optical pumping. We point out that all but the ground rotational state obtains a vanishing low-frequency scalar polarizability from coupling with adjacent rotational states, because of a fortuitous relationship between rigid rotor spacings and dipole matrix elements. We project that, for good choices of spectroscopy states, demonstrated levels of field control should make possible uncertainties of order  $1 \times 10^{-18}$ , similar to those of leading atomic ion clocks. If fast state preparation can be achieved, the moderately long-lived vibrational states of  $\text{TeH}^+$  make possible a frequency uncertainty approaching  $1 \times 10^{-17}$  with one day of averaging for a single trapped ion. Observation over one year could probe for variation of  $\mu$  with a sensitivity approaching the  $1 \times 10^{-18}/\text{yr}$  level.

DOI: [10.1103/PhysRevA.98.052513](https://doi.org/10.1103/PhysRevA.98.052513)**I. INTRODUCTION**

Searches for variation of fundamental constants are motivated by their ability to probe physics beyond the standard model [1]. Modern laboratory searches for variation use precise frequency measurements with sensitivity to the fine-structure constant ( $\alpha$ ) and the proton-electron mass ratio ( $\mu$ ) [2]. Improved searches for variation of  $\mu$  are especially intriguing as it is predicted to drift faster than  $\alpha$  in generic models [3]. If astronomical observations of methanol lines are cast in terms of a linear temporal drift in  $\mu$ , they set a limit of  $2.4 \times 10^{-17}/\text{yr}$  [4]. The tightest laboratory constraint on the fractional variation of  $\mu$ ,  $\sim 1 \times 10^{-16}/\text{yr}$ , was obtained from a comparison of hyperfine and electronic transitions in atomic clocks [5,6], using a shell model calculation to describe the dependence of the nuclear magnetic moment on  $\mu$  [7]. Since the sensitivity to  $\mu$  arises from the relatively low-frequency ( $\sim 10$  GHz) hyperfine transition, it will be challenging to significantly improve the precision of  $\mu$  variation searches by this approach. Vibrational transitions in molecules provide model-independent sensitivity to varying  $\mu$ , with the current best constraint ( $< 5.6 \times 10^{-14}/\text{yr}$ ) obtained in a molecular beam [8].

Spectroscopy on single trapped atomic ions has achieved statistical and systematic uncertainties at the low  $10^{-18}$  level [9,10]. Recent demonstrations of molecular-ion quantum state preparation [11–15] and nondestructive readout [15,16] suggest that spectroscopy on a single trapped molecular ion could obtain a high duty cycle in an environment also

favorable for control of systematic uncertainties. In order to evaluate whether this approach to molecular spectroscopy could improve  $\mu$  variation sensitivity beyond the  $10^{-16}$  level of atoms, the intrinsic details of the molecular states and practical aspects of state preparation must be carefully considered. Demonstration of fast optical state preparation for molecular ions with diagonal Franck-Condon factors (FCFs) raises the possibility of small statistical uncertainty for single-molecule spectroscopy [17]. Since other proposed species without diagonal FCFs [18–20] cannot be state prepared by this technique, an investigation of statistical and systematic uncertainties obtainable for a diagonal species like  $\text{TeH}^+$  is of interest.

Compared with hyperfine transitions in atoms, high vibrational overtone intervals (10–1000 THz) of molecules have orders of magnitude larger absolute sensitivity to varying  $\mu$  [21,22]. Optical-frequency single-photon overtone transitions have been observed in trapped molecular ions [23,24]. When the state lifetimes are sufficiently long, such overtone transitions offer a means to surpass the statistical sensitivity of previous searches. One proposed technique is to drive a low-frequency transition from a vibrationally excited state to a nearly degenerate level with different  $\mu$  sensitivity [21,22,25–27]. A challenge of this approach is to find suitable transitions where the dissimilar character of the states does not cause large differential shifts and systematic uncertainties. An alternative approach is to measure the vibrational overtone frequency directly by one-photon [19,28] or two-photon [20,28–32] transitions.

Systematic frequency shifts in polar molecules will generally arise from coupling of nearby rotational and vibrational levels, a serious concern absent in atoms. One response is to

\*b-odom@northwestern.edu

use nonpolar (homonuclear) diatomic molecules, whose vanishing dipole moment eliminates Stark shifts from rotational and vibrational coupling [19,28,31]. However, it is also of great interest to consider polar molecules, particularly since demonstrated optical pumping state preparation techniques require a dipole moment [11,12] or a structure not yet identified in a homonuclear species [14]. Polar molecules have closely spaced levels of opposite parity, which for example allow for molecular orientation in moderate electric fields. One might naively expect that the associated Stark shifts would pose possibly catastrophic challenges for clock-level spectroscopy on polar species. It has previously been pointed out for  $\text{HD}^+$  that the dc scalar polarizability of rotationally excited states is in fact dominated by electronic couplings [33]. Other systematic uncertainties were considered in detail [19,28,34], and it was proposed that a weighted average over a carefully chosen set of disparate transitions could create a composite frequency with a low inaccuracy [19,34]. Here, we point out that the remarkable feature of small dc scalar polarizability actually arises from a nearly precise cancellation of adjacent-level interactions, and that there is a related cancellation of the differential polarizability in the high-frequency limit. Recognizing that the only large polarizabilities unavoidable in polar molecules are tensorial in character, it becomes clear that simple state averaging techniques, known from atomic clocks and previously recognized as being useful for homonuclear spectroscopy [20], can be used to simultaneously suppress this shift as well as linear Zeeman and quadrupole shifts.

## II. MOLECULAR STRUCTURE

We consider the prospects of spectroscopy on a single  $\text{TeH}^+$  ion for an improved search for varying  $\mu$ . Several favorable properties of  $\text{TeH}^+$  stem from its electronic structure, which has been recently computed using multireference configuration interaction with single and double excitations and Davidson correction for higher excitations (MRCISD+Q/aV5Z) calculations [35].

No experimental data are currently available for  $\text{TeH}^+$ , but some confidence in the calculations can be gained by considering the isoelectronic molecule antimony hydride ( $\text{SbH}$ ). Compared with the  $\text{TeH}^+$  calculation, the MRCISD+Q calculation for  $\text{SbH}$  [36] uses a smaller basis set (of quadruple zeta quality) and fewer configuration-state functions and is expected to be less accurate. The experimental data on  $\text{SbH}$  confirm the predictions of the two lowest state symmetries, the cooling transition linewidth to within a factor of 2, and the predictions of low-lying state bond lengths to within 3 pm, which is important for predicting Franck-Condon Factors (FCFs) [37–39]. Further discussion of the reliability of the  $\text{TeH}^+$  calculations can be found elsewhere [17,35]. What would be the implications for this work if theoretical errors are larger than expected? The most significant concerns would be about statistical uncertainties; nondiagonal FCFs could complicate state preparation and shorter vibrational state lifetimes would broaden the spectroscopy transition linewidth. Systematic uncertainties are expected to be fairly robust against theoretical errors, and many of the results of this work would still be quite relevant to this molecule and qualitatively so to other molecules as well.

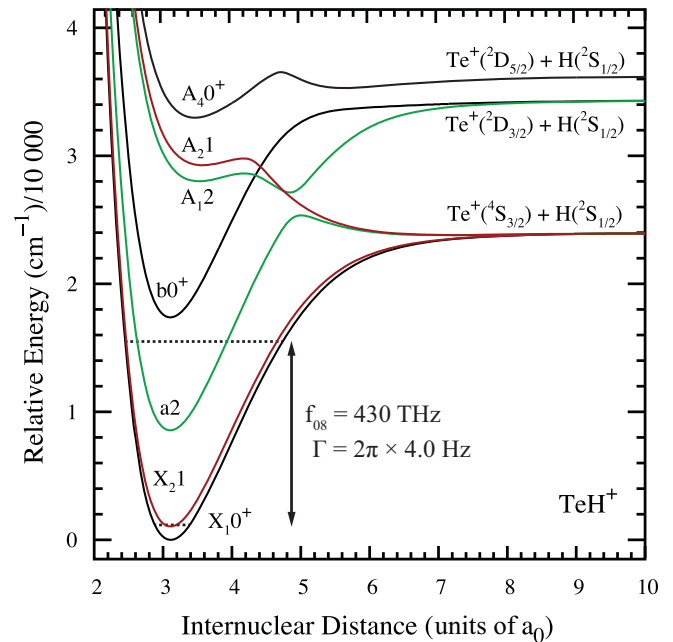


FIG. 1. Relevant low-lying electronic states of  $\text{TeH}^+$ . Dashed lines indicate the initial and final states of the spectroscopy transition,  $v = 0 \rightarrow v' = 8$ , in the  $X_{1,0}^+$  manifold. Figure adapted from [35].

$\text{TeH}^+$  is polar with a predicted ground-state body-frame dipole moment of 0.91 Debye [35]. The lowest few electronic states of  $\text{TeH}^+$  are predicted to have diagonal FCFs [35] (Fig. 1). These diagonal FCFs arise because the states correspond to different orbital and spin configurations of two electrons in nonbonding  $p$  orbitals localized on the tellurium ion, so transitions leave the bond length and strength relatively unperturbed. A diagonal transition from the ground state can make possible rapid spectroscopy state preparation by optical pumping [14], and elsewhere we analyze in detail the prospects for optical state preparation of  $\text{TeH}^+$  [17]. Furthermore, diagonal FCFs reduce shifts arising from the upper spectroscopy state coupling to levels in other electronic manifolds which are close in energy but have poor vibrational overlap.

In the absence of spin-orbit coupling, the  $\text{TeH}^+$  ground state is  $^3\Sigma^-$ , and the two lowest excited states correspond to  $^1\Delta$  and  $^1\Sigma^+$  states [35]. However, strong spin-orbit coupling originating from the heavy tellurium atom makes the Hund's case (c) basis a good approximation to the eigenstates [35,40]. Selection rules that would otherwise prevent transitions between the three lowest-lying  $\Lambda + S$  states are relaxed. The resultant relatively short excited-state lifetimes of the  $b_0^+$  and  $a_2$  states (15  $\mu\text{s}$  and 2.4 ms, respectively, calculated from data from [35] using LEVEL 16 [41]) are important for optical pumping schemes. The ground  $^3\Sigma^-$  state is split into different  $\Omega$  components separated by 1049  $\text{cm}^{-1}$  [35], and we consider spectroscopy transitions within the ( $\Omega = 0$ )  $X_{1,0}^+$  state. We focus on the  $^{130}\text{TeH}^+$  ion, whose lack of Te nuclear spin reduces the complexity of optical pumping. Optical pumping is further simplified because of the relatively large rotational and vibrational constants predicted to be 6.2 and 2100  $\text{cm}^{-1}$ , respectively, arising from the small reduced mass [35]. Larger

level spacings are beneficial for practical optical pumping because fewer states are initially thermally populated, and fewer states are spanned by the spectroscopy transition, after which repumping will be required.  $^{130}\text{TeH}^+$  has  $I = 1/2$ , and we use the Hund's case ( $c_\beta$ ) basis such that  $J_a = L + S$ ,  $J = J_a + R$ , and  $F = J + I$ .

### III. STATISTICAL SENSITIVITY

The sensitivity to varying  $\mu$  of vibrational intervals in homonuclear molecules has previously been considered [21,22,29]. For homonuclear molecules the transition natural linewidth  $\Gamma$  is extremely narrow, and the maximum single-shot probe times are limited by other technical issues such as laser coherence time. Thus choosing an optimal homonuclear spectroscopy interval is free of any intrinsic statistical consideration. In contrast, vibrational state lifetimes of polar hydrides are sufficiently short (typically  $<1$  s) to limit probe times in realistic experiments. Harmonic-oscillator physics provides an estimate for the natural lifetime  $\tau_n$  of the  $n$ th vibrational state, valid for low  $n$ . From  $\langle n-1|x|n\rangle \propto \sqrt{n}$ , we obtain  $\tau_n \approx \tau_1/n$  in the harmonic region. Thus statistical penalties associated with the  $n$ -dependent lifetimes of polar molecule states must be considered. We find below that searches for changing  $\mu$  using polar molecules can benefit from using vibrational overtones rather than the fundamental, but that the relative payoff is weaker than for homonuclears.

In response to a change in  $\mu$ , the fractional change of a vibrational transition from  $v = 0$  to  $v' = n$  at frequency  $\Omega_n$  is given by

$$\frac{\Delta\Omega_n}{\Omega_n} = K_n \frac{\Delta\mu}{\mu}, \quad (1)$$

where we assume here that  $\Omega_n$  is measured by comparing against some clock oscillator with minimal  $\mu$  sensitivity, such as an optical-frequency atomic transition. The relative sensitivity coefficient  $K_n = \partial(\ln\Omega_n)/\partial(\ln\mu)$  describes the fractional response of the transition frequency to varying  $\mu$ . For vibrational fundamental or overtone transitions within the approximately harmonic region,  $K_n \approx -\frac{1}{2}$ , independent of  $n$  [2]. The measured frequency shift itself can be expressed as

$$\Delta\Omega_n = S_n \frac{\Delta\mu}{\mu}, \quad (2)$$

where  $S_n = \Omega_n K_n$  is the absolute sensitivity coefficient of the transition [21,22,29]. For a harmonic oscillator with frequency  $\omega$ ,  $S_n = -n\omega/2$ . Since the strength of the chemical bond does not have leading-order dependence on nuclear masses, the sensitivity must vanish toward dissociation; for a Morse potential the maximum of  $|S_n|$  occurs at roughly 3/4 the dissociation energy [21].

The relative and absolute sensitivity coefficients discussed above do not include any statistical penalty for finite lifetimes of upper states. To take this into account, we define a statistical sensitivity  $\zeta$  given by

$$\zeta_n(T) \equiv \frac{|K_n|}{\sigma_y(T)} = \frac{|S_n|}{\delta\Omega_n(T)}, \quad (3)$$

where  $\sigma_y(T) = \delta\Omega_n(T)/\Omega_n$  is the Allan deviation for some overall measurement time  $T$  and  $\delta\Omega_n(T)$  is the associated frequency uncertainty. There are two physical interpretations for  $\zeta_n(T)$ . First, it gives the ratio of frequency shift to frequency uncertainty, for some fractional change in  $\mu$ :

$$\frac{\Delta\Omega_n}{\delta\Omega_n(T)} = \zeta_n(T) \frac{\Delta\mu}{\mu}. \quad (4)$$

Alternatively, the frequency measurements provide a measurement of the quantity  $\mu$  itself (albeit with very large theoretical uncertainty) and the square root of the two-sample variance is given by  $\sigma_y^{(\mu)}(T) = \zeta_n^{-1}(T)$ .

For a projection-noise limited Ramsey-style measurement on a single ion, the rms error is given by

$$\delta\Omega_n(T) = \frac{1}{T_R C} \sqrt{\frac{T_c}{2T}}, \quad (5)$$

where  $T_R$  is the Ramsey time,  $T_c$  is the cycle time,  $T$  is the total measurement time, and  $C$  is the fringe visibility (e.g.,  $C = 0.6$  for  $T_R = \tau_n$ ) [42,43]. We can then express how the statistical uncertainty scales with choice of vibrational overtone:

$$\delta\Omega_n(T) = \left(\frac{\tau_1}{\tau_n}\right)^k \delta\Omega_1(T), \quad (6)$$

with  $0 \leq k \leq 1$ . The particular value of  $k$  depends on the relationship between  $T_R$ ,  $T_c$ , and  $\tau$  in the measurement protocol. We consider three limiting cases: (1)  $k = 0$  for  $T_R, T_c \ll \tau$ , most relevant to homonuclear spectroscopy, (2)  $k = 1$  for  $T_R = \tau$  and  $T_R \ll T_c$ , representing dead time limited cycling relevant to polar molecule spectroscopy, and (3)  $k = \frac{1}{2}$  for  $T_R = \tau$  and  $T_c = 2T_R$ , representing optimal cycling for any molecule. Although it would be statistically preferable to have the longer upper-state lifetimes of homonuclears, a sort of consolation for polar hydride spectroscopy is that their moderate lifetimes can in some cases allow  $k = \frac{1}{2}$  to be approached using optical pumping techniques [14,17].

The statistical sensitivities  $\zeta_n(T)$  and  $\zeta_1(T)$  are then related by

$$\zeta_n(T) = \frac{|S_n|}{|S_1|} \left(\frac{\tau_n}{\tau_1}\right)^k \zeta_1(T). \quad (7)$$

For a harmonic oscillator, the sensitivity and lifetime scalings discussed above yield (1)  $\zeta_n(T)/\zeta_1(T) = n$  for  $k = 0$ , (2)  $\zeta_n(T)/\zeta_1(T) = 1$  for  $k = 1$ , and (3)  $\zeta_n(T)/\zeta_1(T) = n^{1/2}$  for  $k = \frac{1}{2}$ . The strongest benefit of increasing  $n$  occurs for the  $k = 0$  case, most relevant to homonuclear spectroscopy.

Reference [35] predicts  $\text{TeH}^+ X_1 0^+$  vibrational state spontaneous emission lifetimes spanning from 200 ms down to 20 ms, over the frequency range 60–600 THz. Stimulated emission from blackbody radiation at room temperature will be orders of magnitude slower. In Fig. 2 we plot the  $\text{TeH}^+$  statistical sensitivity for the three limiting cases of  $k$ , as a function of excited vibrational state. Nontrivial dipole moment functions and reduced anharmonic level spacings [35] contribute to the slight enhancement at low  $n$  of the sensitivity ratio, as compared with the harmonic-oscillator values. The statistical uncertainty for the linewidth-limited  $k = \frac{1}{2}$  case is minimized using the overtone  $\Omega_8/(2\pi) = 430$  THz with  $\tau_8 = 40$  ms. Averaging yields  $\delta\Omega_8(T)/\Omega_8(T) =$

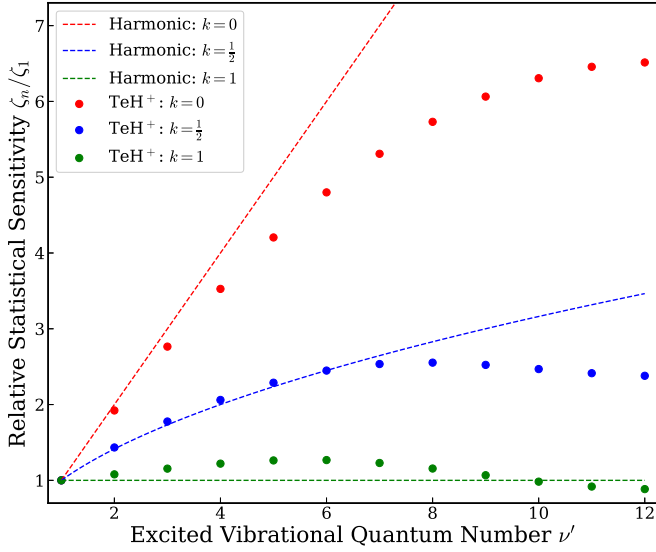


FIG. 2. Statistical sensitivity to  $\mu$  of  $\text{TeH}^+$  overtone transitions  $\Omega_n$ , relative to that of the vibrational fundamental transition  $\Omega_1$ . Values of  $k$  correspond to different experimental timing cases, described in the text. The dashed curves show the harmonic-oscillator values.

$3.1 \times 10^{-15}/\sqrt{T/s}$ , or  $1.0 \times 10^{-17}$  at 1 day, corresponding to  $\delta\Omega_8/(2\pi) = 4.3$  mHz. The corresponding sensitivity coefficients are  $K_8 = -0.40$ ,  $S_8 = 2\pi \times 170$  THz, and  $\zeta_8(1 \text{ day}) = 4.0 \times 10^{16}$ , with  $\sigma_y^{(\mu)}(1 \text{ day}) = 2.5 \times 10^{-17}$ . It is important to note that approaching this best-case statistical uncertainty requires state preparation significantly faster than the upper spectroscopy state lifetime. In Ref. [17] we find that the 15  $\mu\text{s}$  lifetime of the  $b0^+$  state should allow for rapid optical state preparation, such that  $k = \frac{1}{2}$  can be approached.

#### IV. POLARIZABILITY CALCULATIONS

We compute  $\text{TeH}^+$  Stark shifts directly from the Hamiltonian, without actually using expressions for polarizabilities. However, since we find that some shifts vanish when averaged over  $M_F$ , a description in terms of scalar and tensor polarizabilities is suggested, and this description is also helpful for comparing behavior of different species. We take the quantization axis  $\hat{z}$  to be defined along the direction of an applied magnetic field, and all electric fields we consider are relatively small such that Stark shifts are much smaller than the Zeeman intervals. In this case, the Stark shift can be expressed as

$$\Delta W = -\frac{1}{2} E_{\text{rms}}^2 \left[ \alpha_S(\omega) + D \alpha_T(\omega) \frac{3M_J^2 - J(J+1)}{(2J-1)(2J+3)} \right], \quad (8)$$

where  $E_{\text{rms}}$  is the rms value of the oscillating field polarized along  $\hat{\mathbf{u}}$ ,  $D = (3|\hat{\mathbf{u}} \cdot \hat{\mathbf{z}}|^2 - 1)$ , and  $\alpha_S$  and  $\alpha_T$  are the dynamic scalar and tensor polarizabilities [44,45]. [Note that we have defined  $\alpha_T$  using the molecular convention, which causes the  $M_J$ -dependent factor to be  $(2J)/(2J+3)$  times that of the atomic convention.] This expression has the correct form in the dc limit where  $E_{\text{dc}} = E_{\text{rms}}$ . Since the second term in Eq. (8) vanishes when summed over polarizations, as occurs naturally for an isotropic blackbody radiation (BBR)

field, or when measured spectra are averaged over Zeeman states, effects of the tensor polarizability can be strongly suppressed [46,47]. The scalar polarizabilities are of greater concern.

If the rotational energy spacing is relatively small, then expressions of the same form as Eq. (8) can be written for polarizabilities arising from coupling to adjacent rotational levels ( $\alpha^r$ ), adjacent vibrational manifolds ( $\alpha^v$ ), the spin-orbit split  $X_21$  manifold ( $\alpha^{\text{SO}}$ ), and electronically excited manifolds ( $\alpha^e$ ), such that

$$\Delta W = \Delta W^r + \Delta W^{\text{SO}} + \Delta W^v + \Delta W^e. \quad (9)$$

#### A. Polarizability formalism for $J$ states

We first consider the case of zero nuclear spin. In the approximation that (1) the rotational spacing is small compared with other intervals and (2) electronic and vibrational transition dipole moments do not change significantly when the rovibrational wave function  $v(J)$  is replaced with  $v(J')$  for  $J' = J \pm 1$ , then the (orientation-dependent) individual terms for  $\Omega = 0$  states can be written as

$$\begin{aligned} \Delta W^x(\gamma, J, M_J) &= -\frac{1}{2} E_{\text{rms}}^2 \left[ \alpha_S^x(\gamma, J; \omega) + D \alpha_T^x(\gamma, J; \omega) \frac{3M_J^2 - J(J+1)}{(2J-1)(2J+3)} \right], \end{aligned} \quad (10)$$

with  $D = (3|\mathbf{u} \cdot \mathbf{z}|^2 - 1)$  and  $x \in \{r, \text{SO}, v, e\}$  [44]. We have again used the standard convention for defining the molecular  $\alpha_T$ , in which the  $M_J$ -dependent multiplier in Eq. (10) is  $(2J)/(2J+3)$  times that of the atomic convention. With these definitions, Ref. [44] shows that for  $I = 0$  the electronic polarizabilities have the following relations:

$$\begin{aligned} \alpha_S^e &= \frac{1}{3} [\alpha_{\parallel} + 2\alpha_{\perp}], \\ \alpha_T^e &= \frac{2}{3} [\alpha_{\parallel} - \alpha_{\perp}]. \end{aligned} \quad (11)$$

Here,  $\alpha_{\parallel}$  and  $\alpha_{\perp}$  are the electronic polarizabilities associated with  $\Delta\Omega = 0$  and  $\Delta\Omega \pm 1$  transitions and  $(\alpha_{\parallel} - \alpha_{\perp})$  is known as the polarizability anisotropy.

The second-order perturbation expression for the Stark shifts of a state  $|\gamma, J, M_J\rangle$  coupled to a manifold  $\gamma'$  by an oscillating electric field  $\mathbf{E}(t) = \mathcal{E} \cos \omega t \hat{\mathbf{z}}$  is given by

$$\begin{aligned} \Delta W^x(\gamma, J, M_J) &= \sum_{J'} \frac{E_{\text{rms}}^2 |\langle \gamma, J, M_J | d_z | \gamma', J', M_J \rangle|^2}{\hbar} \\ &\quad \times \frac{-\Delta}{\Delta^2 - \omega^2}, \end{aligned} \quad (12)$$

where  $d_z$  is the laboratory-frame  $z$  component of the dipole operator,  $\hbar\Delta$  is the signed energy splitting of the states, and  $E_{\text{rms}}$  is the rms field magnitude. In this work, we find the polarizabilities by diagonalizing the Hamiltonian. Combining Eqs. (8) and (12), and recognizing that the tensorial term vanishes when summed over all  $M_J$ , we obtain

$$\alpha_S^x(\gamma, J; \omega) = \sum_{M_J} \sum_{J'} \frac{2|\langle \gamma, J, M_J | d_z | \gamma', J', M_J \rangle|^2}{\hbar(2J+1)} \frac{\Delta}{\Delta^2 - \omega^2}. \quad (13)$$

The tensor polarizability  $\alpha_T^x$  for the manifold can then be found from Eq. (8). For instance, choosing  $M_J = 0$  and  $\mathbf{u} = \mathbf{z}$  we obtain

$$\alpha_T^x(\gamma, J; \omega) = \frac{(2J-1)(2J+3)}{2J(J+1)} \left[ -\alpha_S^x(\gamma, J; \omega) + \sum_{J'} \frac{2|\langle \gamma, J, 0 | d_z | \gamma', J', 0 \rangle|^2}{\hbar} \frac{\Delta}{\Delta^2 - \omega^2} \right]. \quad (14)$$

### 1. Polarizability from adjacent rotational levels

The level spacing for a rigid rotor is  $E_J = B_v J(J+1)$ , yielding an upper energy interval

$$\Delta_{J \rightarrow J+1} = 2(J+1)B_v/\hbar \quad (15)$$

and a signed downward interval

$$\Delta_{J \rightarrow J-1} = -2JB_v/\hbar. \quad (16)$$

For a Hund's case (c) molecule with body-frame dipole moment  $\mu_0$  in a  $z$ -polarized field, the polarizability due to coupling to adjacent rotational levels, from Eq. (8) and, e.g., Ref. [40], becomes

$$\alpha_S^r(\omega) = \sum_{M_J} \sum_{J'} \frac{2|\langle \gamma, J, M_J | -\mu_z | \gamma', J', M_J \rangle|^2}{\hbar(2J+1)} \frac{\Delta_{JJ'}}{\Delta_{JJ'}^2 - \omega^2} \quad (17)$$

$$= 2\mu_0^2 \sum_{M_J} \sum_{J'} (2J'+1) \left| \begin{pmatrix} J & 1 & J' \\ -M_J & 0 & M_J \end{pmatrix} \begin{pmatrix} J & 1 & J' \\ -\Omega & 0 & \Omega \end{pmatrix} \right|^2 \frac{\Delta_{JJ'}}{\Delta_{JJ'}^2 - \omega^2}. \quad (18)$$

We use

$$\begin{pmatrix} J+1 & 1 & J \\ -M_J & 0 & M_J \end{pmatrix} = (-1)^{J-M_J+1} \left[ \frac{2(J+M_J+1)(J-M_J+1)}{(2J+1)(2J+2)(2J+3)} \right]^{1/2} \quad (19)$$

and for  $\omega \ll \Delta$

$$\frac{\Delta_{JJ'}}{\Delta_{JJ'}^2 - \omega^2} \approx \frac{1}{\Delta} \left( 1 + \frac{\omega^2}{\Delta^2} \right). \quad (20)$$

As an example, taking  $\Omega = 0$ ,  $J' = 1$  for  $J = 0$  or  $J' = J \pm 1$  for  $J \geq 1$ , for the low-frequency limit  $\omega \ll \Delta$  we obtain

$$\alpha_S^r(\omega) \approx \begin{cases} \left( \frac{\mu_0^2}{3B_v} \right) \left[ 1 + \left( \frac{\hbar\omega}{2B_v} \right)^2 \right] & \xrightarrow{\omega \rightarrow 0} \frac{\mu_0^2}{3B_v}, \quad J = 0, \\ \left( \frac{\mu_0^2}{3B_v} \right) \left( \frac{1}{J(J+1)} \right)^2 \left( \frac{\hbar\omega}{2B_v} \right)^2 & \xrightarrow{\omega \rightarrow 0} 0, \quad J \geq 1. \end{cases} \quad (21)$$

The cancellation for  $J \geq 1$  states occurs because the interactions with the next-lower and next-higher states cancel each other. This is a nontrivial result, since the level spacing and coupling strengths are different for each interval. We find empirically that this cancellation holds for other molecular configurations, including  $\Omega \neq 0$  in Hund's case ( $c_\beta$ ) and Hund's cases (a) and (b). (Note that for some of these cases there is  $\Lambda$  or  $\Omega$  doubling, and the polarizability arising from coupling of the doublet states is finite.)

This result is consistent with the null value obtained when one averages over  $M_J$  the well-known expressions for rigid rotor Stark shifts in  $^1\Sigma$  molecules [40,48], with the previous observation that the  $M_J$ -averaged dc polarizability vanishes for  $J > 0$  in  $^1\Sigma$  molecules [49], and with calculations showing that  $\alpha_S^e(0)$  for the  $^2\Sigma^+$  molecule  $\text{HD}^+$  is dominated by  $\alpha_S^e(0)$  [33]. Deviations from the rigid-rotor energy spectrum approximation are discussed in Sec. V.

One can also show that in the limit  $\omega \gg B_v/\hbar$  rotational coupling causes all levels except for  $J = 1/2$  to obtain a common scalar polarizability  $\alpha_S = -\frac{4\mu_0^2 B_v}{3\hbar^2 \omega^2}$ . This result is relevant, for instance, for Stark shifts from BBR coupling

of rotational levels. However, in practice, since these shifts are small, this cancellation is less important than the low-frequency case.

### 2. Polarizability from unbound electronic levels

For computing the polarizability from coupling to the unbound  $A_21$  level, we use a "classical" approximation which takes the classical position and momentum of the spectroscopy state as a function of internuclear distance  $R$  and uses the requirement of conservation of nuclear position and momentum to define a single energy in the excited potential which is coupled. It is easily shown that the coupling interval is given by the so-called difference potential  $\Delta V(R)$ , the interval between the two potential-energy curves [50–53]. Then the frequency shift in response to an off-resonant field is given by

$$\Delta f = \int dR \Delta f(\mu(R), \Delta V(R), E(t)) |\Psi(R)|^2, \quad (22)$$

where  $\Psi(R)$  is the nuclear wave function,  $\mu(R)$  is the laboratory frame transition moment, and  $\Delta f(\mu, \Delta E, E(t))$  describes the light shift for driving field  $E(t)$  of a level

TABLE I. Contributions to scalar and tensor dc polarizabilities and 300 K BBR shifts for selected  $X_10^+$  states. For simplicity, we present here  $J$ -state  $|v, J\rangle$  values. The proposed spectroscopy transition is marked with an asterisk. Tensor polarizabilities use the molecular prefactor convention described in the text.

|                  | $\alpha_S(\omega = 0)$ (a.u.) |              |                 |              | $\alpha_T(\omega = 0)$ (a.u.) |              |                 |              | $\Delta_{300}$ (mHz) |                  |                     |                  |
|------------------|-------------------------------|--------------|-----------------|--------------|-------------------------------|--------------|-----------------|--------------|----------------------|------------------|---------------------|------------------|
|                  | $\alpha_S^r$                  | $\alpha_S^v$ | $\alpha_S^{so}$ | $\alpha_S^e$ | $\alpha_T^r$                  | $\alpha_T^v$ | $\alpha_T^{so}$ | $\alpha_T^e$ | $\Delta_{300}^r$     | $\Delta_{300}^v$ | $\Delta_{300}^{so}$ | $\Delta_{300}^e$ |
| $ 0, 0\rangle$   | 1500                          | 0.02         | 0.04            | 1            | 0                             | 0            | 0               | 0            | 12                   | -0.2             | -0.4                | -10              |
| $ 0, 1\rangle^*$ | 0.08                          | 0.02         | 0.04            | 1            | 1100                          | -0.04        | 0.02            | 0.6          | 11                   | -0.2             | -0.2                | -10              |
| $ 0, 2\rangle$   | 0.2                           | 0.02         | 0.04            | 1            | 400                           | -0.04        | 0.02            | 0.6          | 11                   | -0.2             | -0.2                | -10              |
| $ 8, 2\rangle^*$ | 0.3                           | -0.03        | 0.03            | 0.6          | 600                           | -0.09        | 0.01            | 0.3          | 11                   | 0.4              | -0.1                | -6               |

coupled by transition moment  $\mu$  to another level separated in energy  $\Delta E$ . The results we obtain by integrating over  $|\Psi(R)|^2$  are similar to what we obtain by a simple turning point approximation. Lab frame transition moments are obtained from rotationless transition moments in the usual way, the shifts are summed over coupled  $F'$ ,  $M'_F$  levels, and scalar and tensorial polarizabilities are extracted as described previously.

### B. Polarizability formalism for $F$ states

When comparing differential polarizabilities with those of atoms, it is important to consider the  $F$  states. It can be shown for atoms that the polarizability for  $F$  states can be written in the same form as Eq. (8), but with  $J \rightarrow F$  and  $M_J \rightarrow M_F$  [45]. Since we are considering Hund's case ( $c_\beta$ ), where  $F = J + I$ , the same arguments apply to  $\text{TeH}^+$ .  $F$ -state polarizabilities are calculated by first finding the numerical Stark shifts and then solving the equations for  $\alpha_S(\gamma, F; \omega)$  and  $\alpha_T(\gamma, F; \omega)$ .

## V. ASSESSMENT OF $\text{TeH}^+$ STARK SHIFTS

Stark shifts and polarizabilities are calculated according to the formalism described above, using dipole moment functions from [35]. Low-frequency polarizability results are presented in Table I, and the BBR shifts shown in Table I encapsulate the most important consequence of high-frequency polarizability. Comparison of these values with those of optical atomic clock polarizabilities are given in Table II, and projected Stark shift uncertainties are in Table IV. Light shifts are discussed in Sec. VE.

TABLE II. Comparison of  $\text{TeH}^+ |v = 0, J = 1, F = 1/2\rangle \rightarrow |v=8, J = 2, F=3/2\rangle$  and atomic ion clock transition parameters [9,55–57]. Differential shift coefficients are given for dc polarizabilities  $\Delta\alpha(0)$ , 300 K BBR Stark shift  $\Delta f_{300}$ , quadratic Zeeman shift  $\Delta_{M_2}$ , and quadrupole shift  $\Delta\Theta$ , all computed for the  $F$  states of the transition. For comparison tensor polarizabilities here use the atomic convention, denoted  $\alpha_T^{(a)}$ , so  $\text{TeH}^+$  values are smaller than those of Table I by a factor of  $2J/(2J + 3)$ .  $\Delta\alpha$  and  $\Delta\Theta$  are the differences between the upper- and lower-state values. Lower- and upper-state linear Zeeman shifts are given by the  $g$  factors  $g_g$  and  $g_e$ , where  $E = gm_F\mu_B$ . The quadratic Zeeman coefficient  $\Delta_{M_2}$  is either for  $m_F = 0 \rightarrow m'_F = 0$  or for an average over Zeeman components effectively creating that transition. The statistical uncertainty  $\delta f/f$  is for 1 day of averaging, with  $T_R$  set to the upper-state lifetime for  $\text{TeH}^+$  and  $\text{Sr}^+$  and  $T_R^*$  set to a laser coherence time of 6 s [58] for  $\text{Al}^+$  and  $\text{Yb}^+$ .

|                               | $\Delta\alpha_S(0)$ (a.u.) | $\Delta\alpha_T^{(a)}(0)$ (a.u.) | $\Delta f_{300}$ (Hz) | $g_g$   | $g_e$  | $\Delta_{M_2}$ (Hz/mT <sup>2</sup> ) | $\Delta\Theta$ (a.u.) | $\delta f/f \times 10^{18}$ |
|-------------------------------|----------------------------|----------------------------------|-----------------------|---------|--------|--------------------------------------|-----------------------|-----------------------------|
| $\text{TeH}^+$ (430 THz)      | -0.4                       | 250                              | 0.005                 | 0.07    | 0.05   | 40 000                               | 0.3                   | 10                          |
| $\text{Al}^+$ (1100 THz)      | 0.5                        | 0                                | -0.004                | -0.0008 | -0.002 | -70                                  | 0                     | 0.3*                        |
| $\text{Sr}^+$ (445 THz)       | -30                        | -50                              | 0.2                   | 2       | 1      | 3                                    | 3                     | 3                           |
| $\text{Yb}^+$ $E_2$ (688 THz) | 50                         | -70                              | -0.4                  |         | 0.8    | 50 000                               | 2                     | 6                           |
| $\text{Yb}^+$ $E_3$ (642 THz) | 5                          | -1                               | -0.04                 |         | 1      | -2000                                | -0.04                 | 0.6*                        |

Since understanding the general Stark shift properties of the molecule does not require introducing nuclear spin, for simplicity we present in Table I the polarizabilities and BBR shifts for the case of  $I = 0$ , i.e., for  $J$  states. However, for our calculations of systematic shifts in Table IV, we use the Stark shifts for the actual  $F$  states.

### A. Electronic polarizability

To anticipate the magnitude of electronic polarizabilities from the potential-energy curves (Fig. 1), it is important to recognize that the vibrational wave functions generally cause the upper spectroscopy state to couple to other electronic manifolds well above their minimum energies. Polarizabilities are calculated for couplings to the  $X_21$ ,  $b0^+$ ,  $A_12$ , and  $A_21$  states. Since transition moments to other electronic states are small [35], they are not expected to contribute significantly to the polarizability. Polarizabilities arising from coupling to different spin-orbit states are also small, owing to small transition moments.

### B. Vibrational polarizability

Because the rotational and vibrational spacing is much smaller than the electronic spacing,  $\alpha^v(\omega)$  or  $\alpha^r(\omega)$  for polar molecules might be expected to dominate the differential Stark shift at low frequencies and also to play a significant role at high frequencies. For the case of  $\alpha^v(\omega)$ , this turns out to not normally be the case, for straightforward reasons. Vibrational transition moments for polar hydrides are typically  $\leq 10\%$  of electronic transition moments, so, after squaring to obtain the

Stark shift, vibrational contributions to Stark shifts are still smaller than electronic contributions despite the closer level proximity.

### C. Rotational polarizability

The case of polarizability from rotational coupling is much more interesting. As discussed in Sec. IV A 1, we find that the relationship between the rigid-rotor level spacings and corresponding dipole matrix elements essentially eliminates effects of  $\alpha_S^r$ . In the low-frequency limit, the shifts from the next-lower and next-higher rotational states balance, and  $\alpha_S^r(0) = 0$  for  $J \geq 1$ . Centrifugal distortion has a small effect on the rotational spacing ( $<10^{-4}$  per level for  $\text{TeH}^+$ ) and slightly spoils this cancellation, as can be seen in Table I.

### D. BBR Stark shifts

BBR shifts were calculated by numerically integrating the dynamic Stark shifts over the BBR spectrum [54]. In Table II it is seen that the differential scalar polarizabilities and BBR shifts of  $\text{TeH}^+$  compare favorably with those of atoms. The dominant electronic dipole transition moments in molecules are typically a few times smaller than those in atoms, so it is not surprising that molecular electronic polarizabilities compare favorably. Apart from vanishing for  $J < 1$  (or  $F < 1$ ) states, the molecular  $\alpha_r^r(0)$  is generally large but can be dealt with by averaging over Zeeman levels.

As discussed in Sec. IV A 1, we find in the high-frequency limit that all levels obtain a common  $\alpha_S^r$ , which can be seen in the rotational contributions to BBR shifts in Table I. In practice, this cancellation is not significant for  $\text{TeH}^+$  since the differential electronic BBR shift is relatively large.

In this analysis, we have made the simplifying assumption of an isotropic BBR distribution. In fact, the trap electrodes will modify the BBR field at length scales determined by the trap geometry. Since there is only small BBR spectral density at these length scales, these anisotropies are not expected to significantly modify the predictions shown in Table II. (Note that even for rotational coupling, where the rotational-transition wavelengths are comparable to typical electrode spacings, the Stark shift is dominated by the longer wavelength part of the BBR spectrum.) However, the effects of BBR anisotropies induced by trap electrodes should be the subject of a future study.

### E. Light shifts

When driving a relatively weak overtone transition to an upper state where stronger decay channels are open, the light shift from the spectroscopy laser must be considered. The saturation intensity  $I_{\text{sat}} \propto \Gamma^2/\mu_{\text{eg}}^2$ , where  $\Gamma$  is the total relaxation rate and  $\mu_{\text{eg}}$  is the spectroscopy interval transition moment. Contrary to the two-level case, saturating a weaker (higher) overtone transition  $v = 0 \rightarrow n$  requires increased intensity, since  $\Gamma$  increases with  $n$  but  $\mu_{\text{eg}}$  decreases. For the  $\text{TeH}^+$   $v = 0 \rightarrow 8$  transition, the upper state has  $\Gamma = 25 \text{ s}^{-1}$ , and the spectroscopy channel has  $\Gamma_{80} = 2.4 \times 10^{-4} \text{ s}^{-1}$ , yielding  $I_{\text{sat}} = 1.5 \mu\text{W}/\text{mm}^2$ . At this drive intensity, the estimated differential light shift is 0.5 mHz (a fractional shift of  $1 \times 10^{-18}$ ), dominated by coupling of  $v = 8$  to the  $A_21$  state.

Spectroscopy laser intensity and pointing control can stabilize the shift to below this level.

## VI. ZEEMAN AND QUADRUPOLE SHIFTS

Spectroscopy states within the  $X_10^+$  manifold have intrinsically small linear Zeeman shifts, due to a lack of electronic angular momentum. The remaining moments are of the order of a nuclear magneton. However,  $X_10^+$  acquires some electronic spin via its rotational-electronic coupling with  $X_21$ . This type of mixing, also sometimes called Coriolis coupling, can sometimes significantly affect the spectrum [59–61]. Since the  $\Omega$  doubling in  $X_21$  is primarily caused by rotational-electronic coupling to nearby electronic states of  $\Omega = \pm 1$ , it can be used to estimate the degree of mixing. To determine the linear and quadratic Zeeman shifts, we diagonalize the effective Hamiltonian [40].

### A. Effective Hamiltonian

The effective Hamiltonian [40]

$$\mathcal{H} = \mathcal{H}_{\text{rot}} + \mathcal{H}_{\text{nsr}} + \mathcal{H}_{\text{HFS}} + \mathcal{H}_{Z_I} + \mathcal{H}_{Z_{\text{rot}}} + \mathcal{H}_{Z_S} + \mathcal{H}_E + \mathcal{H}_Q, \quad (23)$$

where  $\mathcal{H}_{\text{rot}}$  is the rotational kinetic energy, and

$$\begin{aligned} \mathcal{H}_{\text{nsr}} &= -c_I T^1(\mathbf{J}) \cdot T^1(\mathbf{I}), \\ \mathcal{H}_{\text{HFS}} &= \mathcal{H}_{\text{HFSb}} + \mathcal{H}_{\text{HFSc}}, \\ \mathcal{H}_{\text{HFSb}} &= b T^1(\mathbf{S}) \cdot T^1(\mathbf{I}), \\ \mathcal{H}_{\text{HFSc}} &= c T_{q=0}^1(\mathbf{S}) \cdot T_{q=0}^1(\mathbf{I}), \\ \mathcal{H}_{Z_I} &= -g_I \mu_N T_0^1(\mathbf{B}) \cdot T_0^1(\mathbf{I}), \\ \mathcal{H}_{Z_{\text{rot}}} &= -g_J \mu_B T_0^1(\mathbf{B}) \cdot T_0^1(\mathbf{J}), \\ \mathcal{H}_{Z_S} &= g_s \mu_B T_0^1(\mathbf{B}) \cdot T_0^1(\mathbf{S}), \\ \mathcal{H}_E &= -T_0^1(\boldsymbol{\mu}_e) \cdot T_0^1(\mathbf{E}), \\ \mathcal{H}_Q &= -T_0^2(\nabla \mathbf{E}) \cdot T_0^2(\mathbf{Q}). \end{aligned} \quad (24)$$

The magnetic field along the laboratory  $\hat{z}$  axis defines the quantization direction. The constants  $c_I$ ,  $g_I$ ,  $g_J$ ,  $g_s$ , and  $\mu_e$  are the nuclear spin-rotation coupling constant, proton  $g$  factor, rotational  $g$  factor, electron spin  $g$  factor, and ground-state body-frame electric dipole moment, respectively. The  $\mathbf{I} \cdot \mathbf{L}$  and  $\mathbf{B} \cdot \mathbf{L}$  terms are omitted since the pure-precession hypothesis is well justified for hydrides [40], in which case  $L$  can be considered a good quantum number with  $L = 0$  for the  $\text{TeH}^+$   $X$  states.

The effective Hamiltonian matrix elements for the  $X_10^+$  and  $X_21$  states are adapted from Ref. [40]. For convenience, the diagonal and off-diagonal components of the rotational Hamiltonian,  $\mathcal{H}_{\text{rot}}^D$  and  $\mathcal{H}_{\text{rot}}^{OD}$ , are separated, where

$\mathcal{H}_{\text{rot}} = \mathcal{H}_{\text{rot}}^D + \mathcal{H}_{\text{rot}}^{OD}$ . The matrix elements are

$$\langle v, J_a; \Omega, J | \mathcal{H}_{\text{rot}}^D | v, J_a; \Omega, J \rangle = B_v [J(J+1) + J_a(J_a+1) - 2\Omega^2],$$

$$\begin{aligned} \langle v, J_a; \Omega, J | \mathcal{H}_{\text{rot}}^{OD} | v, J_a; \Omega' \neq \Omega, J \rangle &= -2B_v (-1)^{J_a - \Omega} \begin{pmatrix} J_a & 1 & J_a \\ -\Omega & q & \Omega' \end{pmatrix} (-1)^{J - \Omega} \begin{pmatrix} J & 1 & J \\ -\Omega & q & \Omega' \end{pmatrix} \\ &\times [J_a(J_a+1)(2J_a+1)J(J+1)(2J+1)]^{1/2}, \end{aligned}$$

where  $q = \Omega - \Omega'$ ,

$$\begin{aligned} \langle v, \Omega, J, I, F | \mathcal{H}_{\text{nsr}} | v, \Omega, J, I, F \rangle &= c_I (-1)^{J+F+I} \begin{Bmatrix} I & J & F \\ J & I & 1 \end{Bmatrix} \times [J(J+1)(2J+1)I(I+1)(2I+1)]^{1/2}, \\ \langle v, J_a; \Omega, J, I, F | \mathcal{H}_{\text{HFSb}} | v, J_a; \Omega', J', I, F \rangle &= b (-1)^{J'+F+I} \begin{Bmatrix} I & J' & F \\ J & I & 1 \end{Bmatrix} [I(I+1)(2I+1)]^{1/2} (-1)^{J-\Omega} \begin{pmatrix} J & 1 & J' \\ -\Omega & q & \Omega' \end{pmatrix} \\ &\times (-1)^{J_a - \Omega} \begin{pmatrix} J_a & 1 & J_a \\ -\Omega & q & \Omega' \end{pmatrix} (-1)^{J_a+L+S+1} \begin{Bmatrix} J_a & S & L \\ S & J_a & 1 \end{Bmatrix}, \end{aligned}$$

where  $q = \Omega - \Omega'$ ,

$$\begin{aligned} \langle v, J_a; \Omega, J, I, F | \mathcal{H}_{\text{HFSc}} | v, J_a; \Omega, J', I, F \rangle &= c (-1)^{J'+F+I} \begin{Bmatrix} I & J' & F \\ J & I & 1 \end{Bmatrix} [I(I+1)(2I+1)]^{1/2} (-1)^{J-\Omega} \begin{pmatrix} J & 1 & J' \\ -\Omega & 0 & \Omega \end{pmatrix} \\ &\times (-1)^{J_a - \Omega} \begin{pmatrix} J_a & 1 & J_a \\ -\Omega & 0 & \Omega \end{pmatrix} (-1)^{J_a+L+S+1} \begin{Bmatrix} J_a & S & L \\ S & J_a & 1 \end{Bmatrix} \times [(2J'_a+1)(2J_a+1)S(S+1)(2S+1)]^{1/2}, \\ \langle v, \Omega, J, I, F, M_F | \mathcal{H}_{Z_{\text{rot}}} | v, \Omega, J, I, F', M_F \rangle &= -g_J \mu_B B_z (-1)^{F-M_F} \begin{pmatrix} F & 1 & F' \\ -M_F & 0 & M_F \end{pmatrix} (-1)^{F'+J+1+I} [(2F'+1)(2F+1)]^{1/2} \\ &\times \begin{Bmatrix} J & F' & I \\ F & J & 1 \end{Bmatrix} [J(J+1)(2J+1)]^{1/2}, \end{aligned} \tag{25}$$

$$\begin{aligned} \langle v, \Omega, J, I, F, M_F | \mathcal{H}_{Z_I} | v, \Omega, J, I, F', M_F \rangle &= -g_I \mu_N B_z (-1)^{F-M_F} \begin{pmatrix} F & 1 & F' \\ -M_F & 0 & M_F \end{pmatrix} (-1)^{F'+J+1+I} [(2F'+1)(2F+1)]^{1/2} \\ &\times \begin{Bmatrix} F & I & J \\ I & F' & 1 \end{Bmatrix} [I(I+1)(2I+1)]^{1/2}, \end{aligned}$$

$$\begin{aligned} \langle v, J_a; \Omega, J, I, F, M_F | \mathcal{H}_{Z_S} | v, J_a; \Omega', J', I, F', M_F \rangle &= g_S \mu_B B_z (-1)^{F-M_F+F'+2J+I+1-\Omega} \begin{pmatrix} F & 1 & F' \\ -M_F & 0 & M_F \end{pmatrix} \begin{pmatrix} J & 1 & J' \\ -\Omega & q & \Omega' \end{pmatrix} [(2F'+1)(2F+1)]^{1/2} \\ &\times [(2J'+1)(2J+1)]^{1/2} \begin{Bmatrix} J & F' & I \\ F' & J' & 1 \end{Bmatrix} (-1)^{J_a - \Omega} \begin{pmatrix} J_a & 1 & J_a \\ -\Omega & q & \Omega' \end{pmatrix} (-1)^{J_a+L+S+1} \\ &\times \begin{Bmatrix} J_a & S & L \\ S & J_a & 1 \end{Bmatrix} [(2J'_a+1)(2J_a+1)S(S+1)(2S+1)]^{1/2}, \end{aligned}$$

where  $q = \Omega - \Omega'$ ,

$$\begin{aligned} \langle v, \Omega, J, I, F, M_F | \mathcal{H}_E | v, \Omega', J', I, F', M_F \rangle &= -\mu_e E_0 (-1)^p (-1)^{F-M_F} \begin{pmatrix} F & 1 & F' \\ -M_F & p & M'_F \end{pmatrix} (-1)^{F'+J+1+I} [(2F'+1)(2F+1)]^{1/2} \\ &\times \begin{Bmatrix} J' & F' & I \\ F & J & 1 \end{Bmatrix} (-1)^{J-\Omega} \begin{pmatrix} J & 1 & J' \\ -\Omega & q & \Omega' \end{pmatrix} [(2J'+1)(2J+1)]^{1/2}, \end{aligned}$$

where  $p$  describes the field polarization, and  $q = \Omega - \Omega'$ ,

$$\begin{aligned} & \langle v, \Omega, J, I, F, M_F | \mathcal{H}_Q | v, \Omega, J', I, F', M_F \rangle \\ &= T_0^2 (\nabla \mathbf{E}) (-1)^{F-M_F} \begin{pmatrix} F & 2 & F' \\ -M_F & 0 & M_F \end{pmatrix} (-1)^{F'+J+2+I} [(2F'+1)(2F+1)]^{1/2} \\ & \times \begin{Bmatrix} J & F & I \\ F' & J' & 2 \end{Bmatrix} (-1)^{J-\Omega} \begin{pmatrix} J & 2 & J' \\ -\Omega & 0 & \Omega \end{pmatrix} [(2J'+1)(2J+1)]^{1/2} \langle v, \Omega | T_0^2(\mathbf{Q}) | v, \Omega \rangle. \end{aligned} \quad (26)$$

Proper definite-parity eigenstates were used for  $\Omega$  doublets in the  $X_21$  manifold. For instance, the parity eigenstate in  $X_21$  coupling to the negative parity  $|v=0, J_a=0; \Omega=0, J=1\rangle$  state will be

$$|v=0, J_a=1; J=1, -\rangle = \frac{1}{\sqrt{2}} (|v=0, J_a=1; \Omega=1, J=1\rangle - |v=0, J_a=1; \Omega=-1, J=1\rangle). \quad (27)$$

We also verified that including Stark couplings at expected stray field levels did not affect the Zeeman shift results.

### B. Estimate of hyperfine constants and rotational $g$ factor

Without any experimental data for  $\text{TeH}^+$ , we must estimate some of the interaction constants, with the values we use listed in Table III. In the case of hydrides, the nuclear spin-rotation coupling  $c_I$  can be somewhat reliably predicted for the heavy atom's nuclear spin-rotation interaction (Eq. 8-41 in [62] or [63]); however, the proton nuclear spin-rotation interaction is both difficult to observe and difficult to predict. We instead estimate the value based on measurements made for molecules possessing a heavy atom both one row below and above tellurium in the Periodic Table. For  $\text{ZnH}$ ,  $c_I(H)$  was measured to be 60 kHz [64], and for  $\text{AuH}$  it was not observed within the experimental uncertainty of 30 kHz [63]. A measurement with similar uncertainty was made for  $\text{AsH}$ , where the value of  $c_I(H)$  was similarly determined to be smaller than the uncertainty [65]. We place a large uncertainty on our estimate of the  $\text{TeH}^+$   $c_I(H)$ , but its effect on the hyperfine splitting is small compared with the other hyperfine parameters. The hyperfine constants  $b$  and  $c$  were estimated from the  $\text{AsH}$  molecule [65], which has very similar electronic structure to  $\text{TeH}^+$ , with As one row above Te in the Periodic Table. The Fermi contact parameter  $b_F$  scales approximately linearly with bond length [66] and the dipolar constant  $c$  scales approximately as the inverse cube of the bond length [67]. Using the ratio of ground-state bond lengths from  $\text{TeH}^+$  to  $\text{AsH}$  of 1.07, we then estimate  $b$  and  $c$  for  $\text{TeH}^+$  from the  $\text{AsH}$  values of  $-53$  MHz and  $13$  MHz, respectively. The rotational  $g$  factor  $g_J$  was estimated from a measurement of  $\text{SbH}$  [68], which has both a very similar reduced mass and electronic structure to that of  $\text{TeH}^+$ . Its small value indicates that the

TABLE III. Constants used in matrix element calculations.

| Constant | Value                       |
|----------|-----------------------------|
| $c_I$    | $\sim 10$ kHz               |
| $b$      | $-50$ MHz                   |
| $c$      | $10$ MHz                    |
| $g_I$    | $5.58$                      |
| $g_J$    | $-0.001$                    |
| $g_s$    | $2$                         |
| $\mu_N$  | $7.62 \times 10^{-4}$ MHz/G |
| $\mu_B$  | $1.40 \times 10^{-4}$ MHz/G |

rotational Zeeman interaction will be the smallest Zeeman term.

### C. Assessment of linear and quadratic Zeeman shifts

Our estimated linear and quadratic Zeeman coefficients are given in Table II. Diagonalization of the effective Zeeman Hamiltonian yields  $X_10^+$  magnetic moments of order  $0.1\mu_B$ . From estimates of the parameters above, we expect a  $J=1/2$  hyperfine splitting of  $\Delta \approx 600$  kHz. The perturbation theory expectation that the  $\text{TeH}^+$  quadratic Zeeman shift is of order  $(g_F M_F \mu_B)^2 / h\Delta$  is in good agreement with the matrix diagonalization result. Compared with  $\text{Yb}^+$ ,  $\text{TeH}^+$  has a significantly smaller magnetic moment but also a much smaller hyperfine spacing. The estimated resulting  $\text{TeH}^+$  quadratic Zeeman shift is similar to that of the  $\text{Yb}^+$  ( $E2$ ) transition and an order of magnitude larger than for the  $\text{Yb}^+$  ( $E3$ ) transition.

### D. Assessment of quadrupole shifts

The quadrupole moment tensor  $T_0^2(\mathbf{Q})$  can be represented in Cartesian coordinates via

$$T_0^2(\mathbf{Q}) = \frac{1}{\sqrt{6}} (2Q_{ZZ} - Q_{XX} - Q_{YY}). \quad (28)$$

Integrating over the internuclear distance  $R$ , the quadrupole moment functions  $Q_{XX}(R)$ ,  $Q_{YY}(R)$ , and  $Q_{ZZ}(R)$  for  $v=8$  in  $X_10^+$  yield  $2.24$ ,  $-1.12$ , and  $-1.12 ea_0^2$ , respectively.

Our proposed spectroscopy transition is discussed further below. The lower state has  $F=1/2$  and no quadrupole shift.

TABLE IV. Projected uncertainty for spectroscopy on  $\text{TeH}^+$   $|v=0, J=1, F=1/2\rangle \rightarrow |v=8, J=2, F=3/2\rangle$ .

| Effect                | $\sigma/f \times 10^{18}$ |
|-----------------------|---------------------------|
| BBR Stark             | 0.9                       |
| dc Stark, scalar      | 0.09                      |
| dc Stark, tensor      | $\ll 1$                   |
| Light shift           | $< 1$                     |
| Quadrupole            | $\ll 1$                   |
| Linear Zeeman         | $< 1$                     |
| Quadratic Zeeman      | 0.6                       |
| Statistics (at 1 day) | 10                        |

For the upper spectroscopy state  $|X_1 0^+, v = 8, J = 2, F = 3/2\rangle$ , we use a calculated quadrupole moment function [69] and the matrix element shown in Eq. (26) to obtain  $\Theta = 0.3ea_0^2$ , which is similar to typical values for atoms. The simple averaging protocol discussed below can be used to effectively eliminate this shift.

## VII. CHOICE OF SPECTROSCOPY TRANSITION

Here we consider some of the options available for spectroscopy on the  $v = 0 \rightarrow v' = 8$  overtone transition of the  $^{130}\text{TeH}^+ X_1 0^+$  electronic state. To leading order the  $J > 0$  states obtain canceling scalar Stark shifts from coupling to the next-lower and next-higher rotational levels, as discussed in Sec. IV A 1. We can then perform spectroscopy on transitions with  $J, J' \geq 1$  without being concerned with large scalar Stark shift associated with the polar character of the molecule. (As an aside, it might appear at first glance attractive to perform spectroscopy on  $F = 1/2$  components of a  $J = 0 \rightarrow J' = 1$  transition, since for these states there is no quadrupole or tensorial Stark shifts. However, the large scalar polarizability of  $J = 0$  makes this transition problematic, since it cannot be reduced by averaging over Zeeman levels. Additionally, the differential quadratic Zeeman shift is large for this transition.)

First-order Zeeman shifts can be strongly suppressed by averaging the  $M_F \rightarrow M'_F$  and  $-M_F \rightarrow -M'_F$  transitions within the manifold [70]. Alternatively, the first-order Zeeman shifts could be reduced by probing  $M_F = 0 \rightarrow M'_F = 0$  transitions in  $^{125}\text{TeH}^+$ , which will also have relatively small quadratic Zeeman shifts due to larger hyperfine splitting [65]. However, since a single-photon  $E1$  transition would not allow for driving from  $F = 0 \rightarrow F' = 0$ , this clock state approach would suffer from the large polar-molecule tensorial Stark shifts that are not averaged away.

Quadratic Zeeman shifts arise from  $M_F$ -preserving mixing between hyperfine states  $F = J \pm I$ . In the ground  $X_1 0^+$  manifold,  $J = 0$  states will have a quadratic Zeeman shift from mixing with  $J = 1$ . The  $J = 1$  and  $J = 2$  manifolds each have a pair of stretched states with  $|M_F| = F = J + 1/2$  possessing small quadratic Zeeman shifts, which might be interesting for precision spectroscopy. However, once again, using exclusively these stretched magnetic sublevel states would not allow for nulling of the large tensorial Stark shift arising from the polar nature of the molecule.

We propose to null tensorial Stark, quadrupole, and linear Zeeman shifts in the same way often done in optical atomic clocks [46,47], by averaging over appropriate combinations of  $M_F \rightarrow M'_F$  with all  $M_F, M'_F$  spanned. We propose using  $J, J' > 0$  to avoid scalar Stark shifts associated with large rotational polarizability of the polar molecule. Specifically, we propose averaging over four spectroscopy transitions:  $|v = 0, J = 1, F = 1/2, M_F = 1/2\rangle \rightarrow |v = 8, J = 2, F = 3/2, M_F = 1/2(3/2)\rangle$  and their negative  $M_F$  partners. These transitions have smaller differential quadratic Zeeman shifts than would transitions involving stretched states.

## VIII. PROJECTED SYSTEMATIC UNCERTAINTIES

Projected limits to experimental precision are given in Table IV. Values are obtained for a bias field of 300 nT, which is more than sufficient to resolve the Zeeman components. We use a magnetic-field instability of 10 nT, which is a few times worse than achieved in [71]. We use an electric-field uncertainty of 100 V/m, which is not the best achieved in single-ion experiments [72] but is similar to the level arising in a two-ion experiment where uncontrolled dc fields of up to 10 V/m [73] push the ions off axis into a finite rf field. Finally, for quadrupole shifts, we use the axial gradient of our trap of 30 V/mm<sup>2</sup> and conservatively assume an uncertainty in this gradient of 1%.

The BBR uncertainty is from a 5 K temperature stability at 300 K. Light shifts are discussed in Sec. V E. The low-frequency scalar Stark shift uncertainty arises directly from the uncontrolled rf fields described above. We rely on suppression of the tensorial Stark shift by the  $M_F$  averaging techniques discussed above, which have been used to suppress tensorial Stark shifts by four orders of magnitude [74]. A suppression by 1000 would make these shifts similar in magnitude to the scalar Stark shifts. Similarly, we project a quadrupole shift uncertainty from the field gradient uncertainty discussed above and a suppression factor of 1000 from  $M_F$  averaging.

The proposed technique of suppression of linear Zeeman shifts by averaging over opposite pairs of transitions within the spectroscopy manifold has achieved suppression of Bohr-magneton sized linear Zeeman shifts at the  $<10^{-17}$  level in a single-ion optical clock [74]. Note that this averaging suppresses the linear Zeeman shift at a level well below that associated with the field uncertainty. Since our differential  $g$  factor is much smaller ( $\Delta g = 0.02$ , discussed in Sec. VI), we project a linear Zeeman uncertainty at  $<10^{-18}$ . The quadratic Zeeman shift cannot be averaged away, and the value in Table IV is what comes directly from the field uncertainty.

## IX. CONCLUSIONS

We have demonstrated the potential for single-photon vibrational overtone spectroscopy on a single polar molecular ion to reach systematic uncertainties at the  $10^{-18}$  level. If a diagonal electronic transition in  $\text{TeH}^+$  can be exploited to obtain rapid state preparation [17], then statistical uncertainties approaching the  $10^{-17}$  level could be obtained for one day of averaging. We conclude that taking measurements over the course of a year could probe for varying  $\mu$  with a sensitivity approaching the  $1 \times 10^{-18}$ /yr level.

The small projected systematic uncertainty comes as somewhat of a surprise, since polar molecules have closely spaced rotational levels which are strongly mixed by low-frequency fields, resulting in large Stark shifts. In this work we point out that the associated polarizability is scalar in character for  $J = 0$  and indeed a significant issue, but that it is tensorial in character for  $J > 0$  and can thus be mitigated by simple averaging protocols regularly used in atomic clocks. The vanishing of this  $J > 0$  dc scalar polarizability arises from a fortuitous relationship between rigid-rotor oscillator strengths and level spacings.

Our results suggest that atoms, polar, and nonpolar molecules can reach similar levels of systematic uncertainty, e.g., they all have electronic polarizabilities which ultimately determine Stark shift uncertainties. However, statistical uncertainties are expected to be quite different. Although homonuclear vibrational state lifetimes are much longer than polar lifetimes, the achievable statistical uncertainty will depend heavily on details of the experimental cycle, such as state preparation time. The spectroscopy cycling rate is a critical issue which could favor polar molecules with diagonal transitions, despite their broader transition linewidths.

Statistical uncertainty will ultimately limit the reach of single-ion spectroscopy on  $\text{TeH}^+$ . To improve the statistical reach of this proposal, the isotopologue  $\text{TeD}^+$  is of interest because it is predicted to have overtone linewidths twice as narrow. Alternatively, the relatively short  $15 \mu\text{s}$  lifetime of the  $\text{TeH}^+$  diagonal  $b0^+-X0^+$  transition might allow fluorescence state readout of multiple ions [75–77]. Performing spectroscopy on a  $|J = 0, F = 1/2\rangle \rightarrow |J = 1, F = 1/2\rangle$  transition would give the ions a negative, albeit large,  $\alpha_S$  which might allow precision spectroscopy on a 2D or 3D crystal with the rf frequency properly tuned such that the Stark and

second-order Doppler shifts cancel [75]. This transition would also be free of tensorial Stark and quadrupole shifts. Finally, we note that the vibrational state lifetimes of  $\text{TeH}^+$  are not particularly long compared with other polar species (e.g., a  $v = 1$  lifetime of 4.0 s in  $\text{CD}^+$  [78] as compared with 0.2 s in  $\text{TeH}^+$ ), so searching for other coolable candidates with favorable properties is well motivated.

## ACKNOWLEDGMENTS

We appreciate computational data on  $\text{TeH}^+$  theory provided by Antonio Gustavo S. de Oliveira–Filho and Fernando R. Ornellas. We thank James Chou and Stephan Schiller for stimulating conversations. B.C.O., M.G.K., and P.R.S. were supported by AFOSR Grant No. FA9550-13-1-0116, NSF Grant No. PHY-1404455, and NSF GRFP No. DGE-1324585. M.K. was supported by a Grant-in-Aid for Scientific Research (B) (Grant No. JP 17H02881), a Grant-in-Aid for Scientific Research (C) (Grants No. JP 17K06483 and No. 16K05500), and a Grant-in-Aid for Exploratory Research (Grant No. JP15K13545) from the Japan Society for the Promotion of Science (JSPS).

- 
- [1] J.-P. Uzan, *Rev. Mod. Phys.* **75**, 403 (2011).  
 [2] P. Jansen, H. L. Bethlem, and W. Ubachs, *J. Chem. Phys.* **140**, 010901 (2014).  
 [3] V. V. Flambaum, D. B. Leinweber, A. W. Thomas, and R. D. Young, *Phys. Rev. D* **69**, 115006 (2004).  
 [4] J. Bagdonaite, M. Dapřa, P. Jansen, H. L. Bethlem, W. Ubachs, S. Müller, C. Henkel, and K. M. Menten, *Phys. Rev. Lett.* **111**, 231101 (2013).  
 [5] R. M. Godun, P. B. R. Nisbet-Jones, J. M. Jones, S. A. King, L. A. M. Johnson, H. S. Margolis, K. Szymaniec, S. N. Lea, K. Bongs, and P. Gill, *Phys. Rev. Lett.* **113**, 210801 (2014).  
 [6] N. Huntemann, B. Lipphardt, C. Tamm, V. Gerginov, S. Weyers, and E. Peik, *Phys. Rev. Lett.* **113**, 210802 (2014).  
 [7] V. V. Flambaum and A. F. Tedesco, *Phys. Rev. C* **73**, 055501 (2006).  
 [8] A. Shelkownikov, R. J. Butcher, C. Chardonnet, and A. Amy-Klein, *Phys. Rev. Lett.* **100**, 150801 (2008).  
 [9] N. Huntemann, C. Sanner, B. Lipphardt, C. Tamm, and E. Peik, *Phys. Rev. Lett.* **116**, 063001 (2016).  
 [10] J.-S. Chen, S. M. Brewer, C. W. Chou, D. J. Wineland, D. R. Leibbrandt, and D. B. Hume, *Phys. Rev. Lett.* **118**, 053002 (2017).  
 [11] P. F. Staunum, K. Højbjerg, P. S. Skyt, A. K. Hansen, and M. Drewsen, *Nat. Phys.* **6**, 271 (2010).  
 [12] T. Schneider, B. Roth, H. Duncker, I. Ernsting, and S. Schiller, *Nat. Phys.* **6**, 275 (2010).  
 [13] A. K. Hansen, O. O. Versolato, Ł. Kłosowski, S. B. Kristensen, A. Gingell, M. Schwarz, A. Windberger, J. Ullrich, J. R. C. López-Urrutia, and M. Drewsen, *Nature (London)* **508**, 76 (2014).  
 [14] C.-Y. Lien, C. M. Seck, Y.-W. Lin, J. H. Nguyen, D. A. Tabor, and B. C. Odom, *Nat. Commun.* **5**, 4783 (2014).  
 [15] C.-w. Chou, C. Kurz, D. B. Hume, P. N. Plessow, D. R. Leibbrandt, and D. Leibfried, *Nature (London)* **545**, 203 (2017).  
 [16] F. Wolf, Y. Wan, J. C. Heip, F. Gebert, C. Shi, and P. O. Schmidt, *Nature (London)* **530**, 457 (2016).  
 [17] P. Stollenwerk, M. Kokish, A. de Oliveira-Filho, F. Ornellas, and B. Odom, *Atoms* **6**, 53 (2018).  
 [18] M. Kajita and Y. Moriwaki, *J. Phys. B: At., Mol., Opt. Phys.* **42** (2009).  
 [19] S. Schiller, D. Bakalov, and V. I. Korobov, *Phys. Rev. Lett.* **113**, 023004 (2014).  
 [20] J.-P. Karr, S. Patra, J. C. J. Koelemeij, J. Heinrich, N. Sillitoe, A. Douillet, and L. Hilico, *J. Phys.: Conf. Ser.* **723**, 012048 (2016).  
 [21] D. DeMille, S. Sainis, J. Sage, T. Bergeman, S. Kotochigova, and E. Tiesinga, *Phys. Rev. Lett.* **100**, 043202 (2008).  
 [22] D. Hanneke, R. A. Carollo, and D. A. Lane, *Phys. Rev. A* **94**, 050101 (2016).  
 [23] J. C. J. Koelemeij, D. W. E. Noom, D. de Jong, M. A. Haddad, and W. Ubachs, *Appl. Phys. B* **107**, 1075 (2012).  
 [24] N. B. Khanyile, G. Shu, and K. R. Brown, *Nat. Commun.* **6**, 7825 (2015).  
 [25] C. Chin and V. V. Flambaum, *Phys. Rev. Lett.* **96**, 230801 (2006).  
 [26] V. V. Flambaum and M. G. Kozlov, *Phys. Rev. Lett.* **98**, 240801 (2007).  
 [27] M. G. Kozlov, *Phys. Rev. A* **80**, 022118 (2009).  
 [28] J. P. Karr, *J. Mol. Spectrosc.* **300**, 37 (2014).  
 [29] T. Zelevinsky, S. Kotochigova, and J. Ye, *Phys. Rev. Lett.* **100**, 043201 (2008).  
 [30] M. Kajita, G. Gopakumar, M. Abe, and M. Hada, *Phys. Rev. A* **85**, 062519 (2012).  
 [31] M. Kajita, G. Gopakumar, M. Abe, M. Hada, and M. Keller, *Phys. Rev. A* **89**, 032509 (2014).  
 [32] M. Kajita, *J. Phys. Soc. Jpn.* **86**, 123301 (2017).  
 [33] S. Schiller, D. Bakalov, A. K. Bekbaev, and V. I. Korobov, *Phys. Rev. A* **89**, 052521 (2014).  
 [34] S. Schiller and V. I. Korobov, *Phys. Rev. A* **98**, 022511 (2018).

- [35] L. Gonçalves dos Santos, A. G. S. de Oliveira-Filho, and F. R. Ornellas, *J. Chem. Phys.* **142**, 024316 (2015).
- [36] A. B. Alekseyev, H.-P. Liebermann, R. M. Lingott, O. Bludský, and R. J. Buenker, *J. Chem. Phys.* **108**, 7695 (1998).
- [37] O. Shestakov, R. Gielen, A. Pravilov, K. Setzer, and E. Fink, *J. Mol. Spectrosc.* **191**, 199 (1998).
- [38] M. Beutel, K. Setzer, O. Shestakov, and E. Fink, *J. Mol. Spectrosc.* **179**, 79 (1996).
- [39] S. Yu, D. Fu, A. Shayesteh, I. E. Gordon, D. R. Appadoo, and P. Bernath, *J. Mol. Spectrosc.* **229**, 257 (2005).
- [40] J. Brown and A. Carrington, *Rotational Spectroscopy of Diatomic Molecules* (Cambridge University Press, Cambridge, UK, 2003).
- [41] R. J. Le Roy, *J. Quant. Spectrosc. Radiat. Transfer* **186**, 167 (2017).
- [42] E. Riis and A. G. Sinclair, *J. Phys. B: At., Mol., Opt. Phys.* **37**, 4719 (2004).
- [43] L. Hollberg, C. W. Oates, E. Anne Curtis, E. N. Ivanov, S. A. Diddams, T. Udem, H. G. Robinson, J. C. Bergquist, R. J. Rafac, W. M. Itano *et al.*, *IEEE J. Quantum Electron.* **37**, 1502 (2001).
- [44] M. Brieger, *Chem. Phys.* **89**, 275 (1984).
- [45] W. M. Itano, *J. Res. Natl. Inst. Stand. Technol.* **105**, 829 (2000).
- [46] P. Dubé, A. A. Madej, J. E. Bernard, L. Marmet, J.-S. Boulanger, and S. Cundy, *Phys. Rev. Lett.* **95**, 033001 (2005).
- [47] P. Dubé, A. A. Madej, Z. Zhou, and J. E. Bernard, *Phys. Rev. A* **87**, 023806 (2013).
- [48] R. D. L. Kronig, *Proc. Natl. Acad. Sci. USA* **12**, 608 (1926).
- [49] M. Cheng, J. M. Brown, P. Rosmus, R. Linguerri, N. Komih, and E. G. Myers, *Phys. Rev. A* **75**, 012502 (2007).
- [50] K. P. Lawley, *Photodissociation and Photoionisation* (John Wiley & Sons, New York, 2009).
- [51] J. Tellinghuisen, *Chem. Phys. Lett.* **99**, 373 (1983).
- [52] J. Tellinghuisen, *J. Chem. Phys.* **80**, 5472 (1984).
- [53] J. Tellinghuisen, in *Advances in Chemical Physics*, Photodissociation and Photoionization, Vol. LX, edited by K. P. Lawley (John Wiley & Sons, New York, 1985), Chap. 7, p. 299.
- [54] J. W. Farley and W. H. Wing, *Phys. Rev. A* **23**, 2397 (1981).
- [55] A. D. Ludlow, M. M. Boyd, J. Ye, E. Peik, and P. O. Schmidt, *Rev. Mod. Phys.* **87**, 637 (2015).
- [56] T. Schneider, E. Peik, and C. Tamm, *Phys. Rev. Lett.* **94**, 230801 (2005).
- [57] C. F. A. Baynham, E. A. Curtis, R. M. Godun, J. M. Jones, P. B. R. Nisbet-Jones, P. E. G. Baird, K. Bongs, P. Gill, T. Fordell, T. Hieta *et al.*, [arXiv:1801.10134](https://arxiv.org/abs/1801.10134).
- [58] M. Bishof, X. Zhang, M. J. Martin, and J. Ye, *Phys. Rev. Lett.* **111**, 093604 (2013).
- [59] A. Carrington, C. A. Leach, A. J. Marr, A. M. Shaw, M. R. Viant, J. M. Hutson, and M. M. Law, *J. Chem. Phys.* **102**, 2379 (1995).
- [60] B. H. McGuyer, C. B. Osborn, M. McDonald, G. Reinaudi, W. Skomorowski, R. Moszynski, and T. Zelevinsky, *Phys. Rev. Lett.* **111**, 243003 (2013).
- [61] M. Borkowski, P. Morzyński, R. Ciuryło, P. S. Julienne, M. Yan, B. J. DeSalvo, and T. C. Killian, *Phys. Rev. A* **90**, 032713 (2014).
- [62] C. H. Townes and A. L. Schawlow, *Microwave Spectroscopy*, Dover Books on Physics (Dover Publications, Mineola, NY, 2013).
- [63] T. Okabayashi, E. Y. Okabayashi, M. Tanimoto, T. Furuya, and S. Saito, *Chem. Phys. Lett.* **422**, 58 (2006).
- [64] F. Tezcan, T. D. Varberg, F. Strohm, and K. M. Evenson, *J. Mol. Spectrosc.* **185**, 290 (1997).
- [65] H. Fujiwara, K. Kobayashi, H. Ozeki, S. Saito, and A. Ismail Jaman, *J. Chem. Soc. Faraday Trans.* **93**, 1045 (1997).
- [66] S. H. Ashworth and J. M. Brown, *J. Chem. Soc. Faraday Trans.* **86**, 1995 (1990).
- [67] J. M. Brown, R. F. Curl, and K. M. Evenson, *J. Chem. Phys.* **81**, 2884 (1984).
- [68] V. Stackmann, K. Lipus, and W. Urban, *Mol. Phys.* **80**, 635 (1993).
- [69] A. G. S. Gonçalves dos Santos and F. R. Ornellas (unpublished).
- [70] T. Nicholson, S. Campbell, R. Hutson, G. Marti, B. Bloom, R. McNally, W. Zhang, M. Barrett, M. Safronova, G. Strouse *et al.*, *Nat. Commun.* **6**, 6896 (2015).
- [71] A. A. Madej, P. Dubé, Z. Zhou, J. E. Bernard, and M. Gertsvolf, *Phys. Rev. Lett.* **109**, 203002 (2012).
- [72] J. Keller, H. L. Partner, T. Burgermeister, and T. E. Mehlstäubler, *J. Appl. Phys.* **118**, 104501 (2015).
- [73] T. Rosenband, D. B. Hume, P. O. Schmidt, C. W. Chou, A. Brusch, L. Lorini, W. H. Oskay, R. E. Drullinger, T. M. Fortier, J. E. Stalnaker *et al.*, *Science* **319**, 1808 (2008).
- [74] P. Dubé, A. A. Madej, A. Shiner, and B. Jian, *Phys. Rev. A* **92**, 042119 (2015).
- [75] K. Arnold, E. Hajiyev, E. Paez, C. H. Lee, M. D. Barrett, and J. Bollinger, *Phys. Rev. A* **92**, 032108 (2015).
- [76] K. J. Arnold and M. D. Barrett, *Phys. Rev. Lett.* **117**, 160802 (2016).
- [77] J. Keller, T. Burgermeister, D. Kalincev, J. Kiethe, and T. E. Mehlstäubler, *J. Phys. Conf. Ser.* **723**, 2 (2015).
- [78] F. R. Ornellas and F. B. C. Machado, *J. Chem. Phys.* **84**, 1296 (1986).